SLAC-PUB-3009
November 1982
(A/I)

MULTIMODE HARMONIC POWER OUTPUT MEASUREMENT OF SLAC HIGH POWER KLYSTRONS*

W. R. Fowkes
Stanford Linear Accelerator Center
Stanford University, Stanford, California 94305
and
E. S. Wu
Institute of Electronics, Klystron Laboratory
Beijing, People's Republic of China

INTRODUCTION

The output power from each of the 244 high power pulsed klystrons at SLAC is routinely measured using thermistor bridge power meters and a sampled signal from a modified Bethe hole directional coupler. These couplers are located in the waveguide coming from each klystron before the four-way power split to each accelerator feed. Adequate low pass filtering has been required since we are primarily interested in the power to the accelerator at its operating frequency of 2856 MHz. Furthermore, one of the properties of the type of directional coupler being used is that there is stronger coupling to higher order modes at higher spurious and harmonically related frequencies. Significant measurement error of the fundamental would result unless low pass filtering is used.

Recently there has been renewed interest at SLAC in the harmonic content of the klystrons. The velocity modulated electron beam within klystron is typically rich in second and third harmonic rf current

---

*Work supported in part by the Department of Energy, contract DE-AC03-76SF00515.

components. The induced current in the output cavity at these frequencies, however, remains weak compared to the fundamental component. There is a reasonably good theory to predict the harmonic rf components of current in the klystron electron beam. These components can typically be 150, 71 and 32 percent for the fundamental, second and third harmonics, respectively, of the dc beam current. Calculating the rf currents induced in the output cavity and subsequent power output at the harmonics is quite difficult, because the output circuit must include parts of the collector and tube body as well, since these chambers are above cutoff as waveguides and suitable boundary conditions for a model cannot be established.

Attempts to calibrate the directional coupler at the lower order harmonics of this operating frequently is useless since there are five propagating modes at the second harmonic and eleven propagating modes at the third harmonic. The degree to which the harmonic (and/or spurious frequency) energy is divided up into the various modes depends both on how the excitation or the initial launching into the waveguide system occurs. It also depends upon mode conversion that takes place due to obstacles and discontinuities such as bends, windows, or vacuum pumpouts ahead of the location that a measurement might be made.

In 1958, M. Forrer and K. Tomiyasu[1] described a movable probe assembly which was used to sample the magnitude and phase of the electric field along both the broad and narrow walls of a pressurized S-band waveguide. The complex field profile was sampled at two different waveguide cross sections. A Fourier analysis on these data by computer enabled the power to be calculated for the various propagating

modes at each frequency. This was done at a power level of 4.7 MW from an S-band magnetron.

Later, V. G. Price[2] made similar measurements using an array of fixed electric probes which were calibrated. Using a computational method similar to Forrer and Tomiyasu, the power in each propagating mode was determined. He shows that, in general, the minimum number of probes required to obtain enough information to determine the power in each mode is slightly greater than the number of modes which can propagate at a given frequency. The accuracy of the measurement is increased if the number of probes is increased beyond the minimum number. This method has the advantage that it is arc free and therefore can be done at higher peak power levels.

About the same time, D. J. Lewis[3] developed a method where a series of mode couplers were designed; each coupler selectively coupling a single mode and discriminating against other modes. This method was useful for measuring second harmonic power where perhaps four or five modes exist, but was impractical for higher frequencies where a large number of modes could propagate.

A few years later, E. D. Sharp and E.M.T. Jones[4] developed a method where the various modes in a large multimode waveguide were discriminately sorted into several smaller dominant mode waveguide arms. This method does not require a computer, but does require an elaborate waveguide discriminator device and must be used where only a limited number of higher order modes can exist. The experimental error is somewhere between ±2 and ±5 db.

The next year J. J. Taub[5] described a method where the power to be measured was fed through a waveguide taper into a much larger, overmoded waveguide and into a large multimode load. The oversized waveguide has an array of 40 or so probes and a line-stretcher ahead of the taper. He shows that the higher mode energy from the standard size waveguide is converted to an approximate plane wave in the overized waveguide. Using filters, the line stretcher, and signals sampled from the various probes, the approximation allows one to determine the total energy at a given frequency to within about ±1 db without knowing how the energy is divided into the various propagating modes.

For our purpose, the movable probe assembly was ruled out because of our high peak power and high vacuum requirements.

The large number of modes at the third harmonic discourage the use of mode selective couplers or the smaller waveguide arms method.

The oversized waveguide method may have been suitable for our purpose, but it required the construction of more elaborate equipment and the purchase of other equipment.

The multiprobe method used by Price seemed the most suitable approach in our situation since much of the required equipment was on hand and the computer capability required (once considered a drawback several years ago) was readily available.

It was decided to confine our investigation to the second and third harmonics of 2856 MHz. To cover the eleven propagating modes at the third harmonic a minimum of eleven probes was required. Price points out that the minimum number of probes required at each broad wall cross section is equal to the highest m-index to occur for a propagating mode.

Since the TE_{40} mode can propagate there will be four probes across the broad wall. The highest n-index determines the number of probes on the narrow wall at each cross section. All the n-indexes are either zero or one, so a single probe at each cross section is adequate. The number of broad wall cross sections required is $1 + N_{max}(1) = 2$. The number of narrow wall cross sections is $1 + M_{max}(1) = 4$. $N_{max}(1)$ is the maximum n-index to occur where the m-index is unity and $M_{max}(1)$ is the maximum m-index to occur for a mode whose n-index is unity.

Four equally spaced probes across the 7.21 cm broad wall placed a constraint on the type of high vacuum rf feedthrough connectors that could be used. The spacing between probe feedthrough connectors and hence the maximum diameter had to be less than about 1.4 cm. This space limitation precluded the use of type N or GR connectors.

The connector/feedthrough assembly chosen was made from a Ceramaseal high vacuum grounded shield connector with a SMA coaxial connector. The feedthrough was brazed into a cupro-nickel cup supplied by us to the manufacturer. This assembly was, in turn, welded into a stainless steel cup which had been brazed into the copper S-band waveguide at the appropriate location. Detail of this feedthrough assembly is shown in Fig. 1. Eleven identical RG 223 double shielded cables connected the somewhat fragile SMA feedthrough probes to a sturdy steel panel with type N bulkhead feedthrough connectors. This panel was securely bolted to a bracket brazed to the copper waveguide assembly. The probe sampling package is shown in Fig. 2.

1. AMPLITUDE AND PHASE CALIBRATION OF PROBE ASSEMBLY

The objective in the probe calibration procedure is to relate the signal measured into a 50Ω termination at the bulkhead panel to the total electric field in the waveguide at the corresponding probe for a given frequency irrespective of the mode. Since it is customary to deal with power ratios in db, further clarification is required.

A pure TE_{10} mode is launched at each harmonic frequency at which the calibration is made. For example, the third harmonic of 2856 MHz is initially launched into WR 90 (standard X-band) waveguide where only the TE_{10} mode can exist and gradually tapered over about ten feet up to WR 284 (standard S-band) waveguide. The power level of the launched wave is measured using a 20 db directional coupler in the X-band waveguide ahead of the taper. The ratio of the power from the i-th probe measured at the bulkhead is compared with the launched TE_{10} power giving:

$$k_i = \frac{P_i}{p^{TE_{10}}} \quad . \tag{1.1}$$

The waveguide probe assembly is terminated with a 100W multimode waveguide termination during the calibration procedure.

The maximum electric field in the matched waveguide for the dominant TE_{10} mode is related to power by

$$G^{TE_{10}} = \frac{P_{10}}{|E_{max}{}^{TE_{10}}|^2} = \frac{ab}{4\eta}\sqrt{1 - (\lambda_0/2a)^2} \tag{1.2}$$

where

a = broad wall dimension,

b = narrow wall dimension,

η = impedance of free space = 377Ω,

λ_0 = free space wavelength at the frequency of interest.

For the dominant TE_{10} mode, the electric field at the i-th probe is related to the maximum electric field by

$$E_{max}^{TE_{10}} \sin(i\pi/p) \tag{1.3}$$

where p is the number of spacing intervals across the waveguide. Thus for four probes equally spaced, p = 5. The i-index is 1, 2, 3 or 4. A probe inconsistent with the regular array but placed at the center would have to be assigned an i-index of 2.5.

Combining Eqs. (1.1), (1.2) and (1.3) gives

$$\frac{P_i}{|E_i|^2} = \frac{G^{TE_{10}} K_i}{\sin^2(i\pi/p)} \tag{1.4}$$

To calibrate the narrow wall probes it was necessary to establish a TE_{01} mode using a suitable taper in height but not width from WR 137 waveguide up to WR 284 waveguide. This mode can propagate at both the second and third harmonics of 2856 MHz. Equations (1.1), (1.2) and (1.3) now have "01" replacing the subscript "10", and "b" replaces "a" under the radical in Eq. (1.2). The narrow wall probes have i = 1 and p = 2.

The characteristic impedance of the probe/feedthrough assemblies turned out to be a poor match to a 50Ω system. It was therefore necessary to use isolators (a different one for each harmonic frequency) in both the probe calibration and the high power measurement.

The analysis also requires that the phase characteristics of each probe and cable assembly be known. If one were able to ensure that the phase shift through each assembly were identical, this part of the calibration procedure would not be necessary. It was found that the calculated phase and the measured phase at the end of each probe cable

varied significantly when the TE_{10} mode was launched for calibration. In both the amplitude and phase calibration, the cables were considered part of the probe assembly.

The phase calibration was made using the system shown in Fig. 3. A Watkins-Johnson M76C double balance mixer was used as the phase detector shown in the figure. Both the second and third harmonics of 2856 are well within the frequency operating range of this device. The calibration including the so-called "dc offset" is different for each frequency. The precision bridge balancing was done using a Hewlett Packard J885A phase shifter for the second harmonic and an HP X885A phase shifter for the third harmonic.

A single wideband signal generator was used for the amplitude and phase calibration for both harmonics. It was necessary to use traveling wave tube amplifiers to obtain adequate calibration signal levels at each of the harmonics.

In principle, it is necessary to know the phase relationship of all of the probes with respect to one another. A straightforward calculation relates all the broad wall probes to each other in the TE_{10} calibration and all the narrow wall probes to each other in the TE_{01} calibration. Of these two probes, however, each have zero field for one or the other of these calibrations using the TE_{10} or TE_{01} modes. Ideally, one could solve this dilemma by launching a pure mode where the phase relationship between the broad and narrow walls is known. Either member of the TE_{11} - TM_{11} degenerate mode pair would be ideally suited for this calibration since phase relationship of the electric field between the broad and the narrow wall is 180° in the former case and 0°

in the latter case. An unsuccessful attempt was made to launch either of these with reasonably good single mode purity. It was decided to assume that the phase shift through each narrow wall probe was the same (for the TM_{11} mode) as the average phase shift of the four broad wall probes in the same waveguide cross section.

2. HIGH POWER MEASUREMENT

The probe assembly was installed at the output of a SLAC XK-5 klystron as shown in block diagram in Fig. 4. A high power load with reasonably good multimode capability was made by terminating a 10-foot long 4 db kanthal coated, water cooled, stainless steel attenuator with a standard SLAC high power water load. The kanthal coated attenuator was built at SLAC for this measurement. The VSWR of this combination load is less than 1.10 for the fundamental mode and less than about 1.6 for all higher order propagating modes at the second and third harmonics.

The power at the fundamental was measured using a directional coupler and a thermistor bridge power meter at the output of the klystron ahead of the multiprobe assembly. The harmonic power levels at the bulkhead panel were measured using an isolator, appropriate band pass filter combinations, and a calibrated HP 8740 broadband crystal detector.

The relative phase of the total electric field at each probe was measured with respect to a constant 10 mw reference which was obtained from a reference probe ahead of the multiprobe assembly. Again, appropriate band pass filter combinations were used in both the signal and reference arms in the phase measurement.

The phase bridge uses a Watkins-Johnson M76C double balanced mixer as a phase detector. Precision phase shifters and attenuators in the waveguide size appropriate to the harmonic being measured are used in the reference and signal arms of the bridge.

After initial setup and checkout, an entire set of amplitude and phase data can be taken in less than an hour. Another hour is required to input the data to the computer.

The measured power output at the fundamental, second and third harmonics for a typical SLAC high power klystron is shown in Table I. The harmonic power is broken down into the various propagating modes.

In this measurement and analysis the minimum number of probes to provide a solution were used. More probes would have reduced the error, especially at the third harmonic. In certain situations a small error in a probe reading could result in a significant error in the final result. In his earlier measurement, Price[2] found that his high power measurements were repeatable within ±1 db in amplitude and ±2° in phase. The measurement technique and the equipment used in the experiment reported herein provided approximately the same repeatability found by Price.

The coupling to the electric field of the probes in the multiprobe assembly turned out to be weaker than perhaps the practical optimum. The trade-off between high signal to noise on the one hand, and the possibility of electrical breakdown and mode conversion on the other, was tilted too far in favor of avoiding the latter. If a second generation probe assembly is to be built at this facility, the probes will have more penetration.

Based on the experience of others[1,2,3,4,5] and on this measurement, the overall accuracy of measuring the power in the various propagating modes on SLAC klystrons is about ±1.5 db.

3. THEORY

The probes will sample the sum of the transverse electric field components for all of the propagating modes. The electric field distribution for any TE_{mn} or TM_{mn} mode have the general form:

$$E_x = E_{xo} \cos\left(\frac{m\pi x}{z}\right) \sin\left(\frac{n\pi y}{b}\right)$$

$$E_y = E_{yo} \sin\left(\frac{m\pi x}{a}\right) \cos\left(\frac{n\pi y}{b}\right) \qquad (2.1)$$

using the coordinate system shown in Fig. 5. Since on the broad wall y is either a or b, then

$$E_y = \pm E_{yo} \sin\left(\frac{m\pi x}{a}\right) \quad , \qquad (2.2a)$$

similarly on the narrow wall

$$E_x = \pm E_{xo} \sin\left(\frac{n\pi y}{b}\right) \quad . \qquad (2.2b)$$

Carrying through the broad wall analysis, the total electric field at any given position x is the sum of the modes which have $m \neq 0$

$$E_{yt}(x) = \sum_m E_{ym} \sin\left(\frac{m\pi x}{a}\right)$$

$$= \sum_m R_m \sin\left(\frac{m\pi x}{a}\right) + j \sum_m I_m \sin\left(\frac{m\pi y}{a}\right) \quad , \qquad (2.3)$$

where

$$E_{ym} = R_m + j\, I_m \quad .$$

The Fourier components R_m and I_m are found as follows: Both sides of Eq. (2.3) are multipled by $\sin(\ell\pi y/a)$ and integrated giving

$$\int_0^a E_{yt}(x) \sin\left(\frac{\ell\pi x}{a}\right) dx = \sum_m \int_0^a E_{ym} \sin\left(\frac{m\pi x}{a}\right) \sin\left(\frac{\ell\pi x}{a}\right) dx \quad . \tag{2.4}$$

Letting $u = \pi x/a$ one obtains

$$\begin{aligned} \frac{a}{\pi}\int_0^\pi E_{yt}(x) \sin\ell u\,du &= \frac{a}{\pi}\sum_m \int_0^\pi E_{ym} \sin mu \sin\ell u\,du \\ &= \frac{a}{\pi}\sum E_{ym}\left[\frac{-\sin(m+\ell)u}{2(m+\ell)} + \frac{\sin(m-\ell)u}{2(m-\ell)}\right]_0^\pi \\ &= \frac{a}{2\pi}\sum E_{ym}\left[\frac{\sin\pi(m-\ell)}{(m-\ell)} - \frac{\sin\pi(m+\ell)}{(m+\ell)}\right] \quad . \end{aligned} \tag{2.5}$$

Since both m and ℓ are integers, the second term in Eq. (2.5) is 0. The first term is π for $m = \ell$ and 0 for all other integers. Therefore,

$$\begin{aligned} \frac{a}{\pi}\int_0^\pi E_{yt}(x) \sin\ell u\,du &= \frac{a}{2}\sum_m E_{ym} \\ &= \frac{a}{2} E_{ym} \qquad (m = \ell) \end{aligned} \tag{2.6}$$

The left-hand side of Eq. (2.4) yields

$$\begin{aligned} \int_0^a E_{yt}(x) \sin\left(\frac{\ell\pi x}{a}\right) dx &= \sum_{i=1}^{p-1} E_{yt}(x_i) \sin\left(\frac{\ell\pi x_i}{a}\right) \Delta x_i \\ &= \sum_{i=1}^{p-1} \frac{a}{p} E_{yt}\left(\frac{ai}{p}\right) \sin\left(\frac{\ell\pi i}{p}\right) \quad , \end{aligned} \tag{2.7}$$

where

$$x_i = ai/p \qquad \Delta x_i = a/p$$

where p represents the number of equally divided segments along the broad wall.

Equation (2.4) becomes

$$\sum_{i=1}^{p-1} \frac{a}{p} E_{yt}\left(\frac{ai}{p}\right) \sin\left(\frac{m\pi i}{a}\right) = \frac{a}{2} E_{ym} \tag{2.8a}$$

therefore

$$E_{ym} = \frac{2}{p} \sum_{i=1}^{p-1} E_{yt}\left(\frac{ai}{p}\right) \sin\left(\frac{m\pi i}{a}\right) \quad . \tag{2.8b}$$

Letting

$$E_{ym} = R_{ym} + jI_{ym} \quad \text{and} \quad E_{yt} = R_{yt} + jI_{yt} \quad ,$$

one obtains the Fourier components R_{ym} and I_{ym}

$$R_{ym} = \frac{2}{p} \sum_{i=1}^{p-1} R_{yt}\left(\frac{ai}{p}\right) \sin\left(\frac{m\pi i}{a}\right) \tag{2.9}$$

$$I_{ym} = \frac{2}{p} \sum_{i=1}^{p-1} I_{yt}\left(\frac{ai}{p}\right) \sin\left(\frac{m\pi i}{a}\right) \tag{2.10}$$

where

$$R_{yt}\left(\frac{ai}{p}\right) = \sum_{m} R_{ym} \sin\left(\frac{m\pi x}{a}\right) \quad , \tag{2.11}$$

$$I_{yt}\left(\frac{ai}{p}\right) = \sum_{m} I_{ym} \sin\left(\frac{m\pi x}{a}\right) \quad . \tag{2.12}$$

For a solution to exist, it is necessary that $m/p < 1$. Therefore, $p \geq 1 + M_{max}$. The larger the value of p, the greater the accuracy. If we set $p = 1 + M_{max}$ where M_{max} is equal to the number of probes across the broad wall at a cross section, we have the following equations

$$E_{yt}\left(\frac{ai}{p}\right) = \left|E_{yt}\left(\frac{ai}{p}\right)\right| \exp(j\phi_{yt}) = R_{yt} + jI_{yt} \tag{2.13}$$

where

$$\tan\phi_{yt} = \frac{I_{yt}}{R_{yt}}$$

and $E_{yt}(ai/p)$ and ϕ_{yt} are measured quantities. The Fourier quantities $|E_{ym}|$ and ϕ_{ym} are determined from

$$|E_{ym}|^2 = |R_{ym}|^2 + |I_{ym}|^2 \tag{2.14}$$

$$\phi_{ym} = \tan^{-1}\left[\frac{I_{ym}}{R_{ym}}\right] \tag{2.15}$$

Only the E_y electric fields, those perpendicular to the broad wall have been treated thus far. For the E_x fields, those perpendicular to the narrow wall, the analysis is identical except that m, a, x and p are replaced, respectively, by n, b, y and q. Similarly, the minimum value of q is $N_{max} + 1$. Again the larger the value of q, the greater the accuracy.

The phase velocities of the propagating modes are all different except for the special case where degenerate mode pairs exist. We must now look at the variation of electric field along the waveguide in the direction of propagation. Specifically, measurements must be made at at least two cross sections in the broad wall and four cross sections in the narrow wall for the eleven propagating modes at the third harmonic.

The electric field quantities E_{ym} expressed previously can be expressed by the complex equation

$$E_{ym} = \sum_n E_{ymn} \tag{2.16}$$

Using the nomenclature and method of Forrer and Tomiyasu, at each measurement cross section one has

$$ {}^{A}E_{ym} = \sum_{n=0}^{n_d} {}^{A}E_{ymn} = {}^{A}R_{ym} + j\,{}^{A}I_{ym} $$

$$ {}^{B}E_{ym} = \sum_{n=0}^{n_d} {}^{B}E_{ymn} = {}^{B}R_{ym} + j\,{}^{B}I_{ym} $$

$$ {}^{C}E_{ym} = \sum_{n=0}^{n_d} {}^{C}E_{ymn} = {}^{C}R_{ym} + j\,{}^{C}I_{ym} $$

$$ \vdots \qquad \vdots \qquad \vdots \qquad \vdots \qquad \vdots \tag{2.17} $$

where A, B, C, ..., refer to respective measurement cross sections at which ${}^{A}E_{m}$, ${}^{B}E_{m}$, ${}^{C}E_{m}$, ..., have been determined. n_d is the highest n-index occurring in the modes under analysis.

Separating Eq. (2.17) into real and imaginary parts one has

$$ {}^{A}R_{ym} = \sum_{n=0}^{n_d} {}^{A}R_{ymn} \qquad {}^{A}I_{ym} = \sum_{n=0}^{n_d} {}^{A}I_{ymn} $$

$$ {}^{B}R_{ym} = \sum_{n=0}^{n_d} {}^{B}R_{ymn} \qquad {}^{B}I_{ym} = \sum_{n=0}^{n_d} {}^{B}I_{ymn} $$

$$ {}^{C}R_{ym} = \sum_{n=0}^{n_d} {}^{C}R_{ymn} \qquad {}^{C}I_{ym} = \sum_{n=0}^{n_d} {}^{C}I_{ymn} $$

$$ \vdots \qquad \vdots \qquad \qquad \vdots \qquad \vdots \tag{2.18} $$

The quantities on the left-hand side of any one of the above equations can be obtained from Eq. (2.16). The right-hand side quantities at the K-th cross section can be related to those at A-th cross section with the transformation equations

$$ {}^{K}R_{mn} = {}^{A}R_{mn} \cos\theta_{mn} + {}^{A}I_{mn} \sin\theta_{mn} $$

$$ {}^{K}I_{mn} = -{}^{A}R_{mn} \sin\theta_{mn} + {}^{A}I_{mn} \cos\theta_{mn} \tag{2.19} $$

where $\theta_{mn} = \beta_{mn}(z_K - z_A)$ is the electrical distance between the two cross sections.

The equations (2.16) are solvable provided $\theta_{mn} \neq 2n\pi$ where n = 0, 1, 2, ... This restriction was taken into account when the distance between waveguide cross sections was selected.

After substituting Eq. (2.19) into (2.18) a linear system of equations with $2(1 + n_d)$ unknowns is obtained. Since the Fourier analysis at each cross section contributes two equations, measurements at $1 + n_d$ cross sections are required. For example, when $n_d = 1$ then measurements are made at $1 + n_d = 2$ cross sections giving

$$
\begin{aligned}
{}^{A}R_{ym} &= \sum_{n=0}^{1} {}^{A}R_{ymn} = {}^{A}R_{ym0} + {}^{A}R_{ym1} \\
{}^{A}I_{ym} &= \sum_{n=0}^{1} {}^{A}I_{ymn} = {}^{A}I_{ym0} + {}^{A}I_{ym1} \\
{}^{B}R_{ym} &= \sum_{n=0}^{1} {}^{B}R_{ymn} = {}^{B}R_{ym0} + {}^{B}R_{ym1} \\
{}^{B}I_{ym} &= \sum_{n=0}^{1} {}^{B}I_{ymn} = {}^{B}I_{ym0} + {}^{B}I_{ym1}
\end{aligned}
\tag{2.20}
$$

From Eqs. (2.19) one obtains

$$
\begin{aligned}
{}^{B}R_{ym0} &= {}^{A}R_{ym0}\cos\theta_{m0} + {}^{A}I_{ym0}\sin\theta_{m0} \\
{}^{B}I_{ym0} &= -{}^{A}R_{ym0}\sin\theta_{m0} + {}^{A}I_{ym0}\cos\theta_{m0} \\
{}^{B}R_{ym1} &= {}^{A}R_{ym1}\cos\theta_{m1} + {}^{A}R_{ym1}\sin\theta_{m1} \\
{}^{B}I_{ym1} &= -{}^{A}R_{ym1}\sin\theta_{m1} + {}^{A}I_{ym1}\cos\theta_{m1}
\end{aligned}
\tag{2.21}
$$

where

$$
\begin{aligned}
\theta_{m0} &= \beta_{m0}(z_B - z_A) \\
\theta_{m1} &= \beta_{m1}(z_B - z_A)
\end{aligned}
\tag{2.22}
$$

Substituting Eqs. (2.21) into (2.20) yields

$$
\begin{aligned}
{}^{A}R_{ym} &= {}^{A}R_{ym0} + {}^{A}R_{ym1} \\
{}^{A}I_{ym} &= {}^{A}I_{ym0} + {}^{A}I_{ym1} \\
{}^{B}R_{ym} &= {}^{A}R_{ym0}\cos\theta_{m0} + {}^{A}I_{ym0}\sin\theta_{m0} + {}^{A}R_{ym1}\cos\theta_{m1} + {}^{A}I_{ym1}\sin\theta_{m1} \\
{}^{B}I_{ym} &= -{}^{A}R_{ym0}\sin\theta_{m0} + {}^{A}I_{ym0}\cos\theta_{m0} - {}^{A}{}_{9}R_{ym1}\sin\theta_{m1} + {}^{A}I_{ym}\cos\theta_{m1}
\end{aligned}
\tag{2.23}
$$

One knows ${}^{A}R_{ym}$, ${}^{A}I_{ym}$, ${}^{B}R_{ym}$ and ${}^{B}I_{ym}$ from cross section measurements and calculations using Eqs. (2.9) and (2.10); θ_{m0} and θ_{m1} are obtained from Eqs. (2.22). Therefore, one can obtain the four unknown quantities ${}^{A}R_{ym0}$, ${}^{A}R_{ym1}$, ${}^{A}I_{ym0}$ and ${}^{A}I_{ym1}$ from the four equations (2.23). Again θ_{m0}, $\theta_{m1} \neq 2n\pi$.

E_{ymn} has now been determined. Note that $E_{ym0} = |E_{ym0}|\exp(j\phi_{m1}$ represents the electric field phasor of the TE_{m0} mode only. The subcomponent $E_{ym1} = |E_{ym1}|\exp(j\phi_{m1})$, however, is the sum of the TE_{m1} and TM_{m1} phasors and therefore is not uniquely associated with a single mode.

The degenerate mode pairs TE_{mn} and TM_{mn} have identical phase velocities and contribute to the electric fields on both the broad and the narrow walls of the waveguide. Separating these degenerate mode pairs may be accomplished by correllating the broad wall and the narrow wall electric fields at the same waveguide cross section. The total field on the waveguide wall is the phasor sum of the TE and TM mode fields so that

$$E_{ymn} = E_y(TM_{mn}) + E_y(TE_{mn}) = R_{ymn} + jI_{ymn} \tag{2.24}$$

$$E_{xmn} = E_x(TM_{mn}) + E_x(TE_{mn}) = R_{xmn} + jI_{xmn} \tag{2.25}$$

The E_x and E_y components are related to one another by

$$E_x(TM_{mn}) = 1/q\ E_y(TM_{mn}) \tag{2.26}$$

$$E_x(TE_{mn}) = -q\ E_y(TE_{mn}) \tag{2.27}$$

where

$$q = \frac{na}{mb} \quad .$$

Eq. (2.24) can be rewritten

$$(R_y^{TM} + jI_y^{TM})_{mn} + (R_y^{TE} + jI_y^{TE})_{mn} = (R_y + jI_y)_{mn}$$

where

$$R_y = R_y^{TM} + R_y^{TE} \tag{2.28}$$

$$I_y = I_y^{TM} + I_y^{TE} \tag{2.29}$$

Substituting Eqs. (2.26) and (2.27) into Eq. (2.25) gives

$$(E_x)_{mn} = 1/q(E_y^{TM})_{mn} - q(E_y^{TE})_{mn} = (R_x + jI_x)_{mn}$$

where

$$R_x = 1/q\ R_y^{TM} - q\ R_y^{TE} \tag{2.30}$$

$$I_x = 1/q\ I_y^{TM} - qI_y^{TE} \quad . \tag{2.31}$$

By first solving the following set of equations

$$R_y = R_y^{TM} + R_y^{TE}$$

$$I_y = I_y^{TM} + I_y^{TE}$$

$$R_x = 1/q\ R_y^{TM} - qR_y^{TE}$$

$$I_x = 1/q\ I_y^{TM} - qI_y^{TE} \quad , \tag{2.32}$$

where R_y, I_y, R_x and I_x are known from measurement and subsequent calcualtion, one obtains four linear equations with unknowns, R_y^{TM}, R_y^{TE}, I_y^{TM} and I_y^{TE} as follows

$$R_y^{TM} = \frac{R_y + (1/q)R_x}{1 + (1/q)^2} \quad , \quad R_y^{TE} = \frac{R_y - qR_x}{1 + q^2}$$

$$I_y^{TM} = \frac{I_y + (1/q)I_x}{1 + (1/q)^2} \quad , \quad I_y^{TE} = \frac{I_y - qI_x}{1 + q^2} \tag{2.33}$$

The maximum electric field amplitudes and phase relationships are

$$|E_y^{TM}|^2 = (R_y^{TM})^2 + (I_y^{TM})^2$$

$$|E_y^{TE}|^2 = (R_y^{TE})^2 + (I_y^{TM})^2$$

$$\phi^{TM} = \tan^{-1}\left[\frac{I_y^{TM}}{R_y^{TM}}\right] \quad , \quad \phi^{TE} = \tan^{-1}\left[\frac{I_y^{TE}}{R_y^{TE}}\right] \tag{2.34}$$

4. DETERMINING THE PROPAGATING POWER IN EACH MODE

The average power in a given mode propagating in the z direction is given by

$$W_z = \frac{1}{2}\int \mathrm{Re}[\bar{E} \times \bar{H}^*]_z d\bar{s} = \frac{1}{2}\int_0^b\int_0^a \mathrm{Re}[E_x H_y^* - E_y H_x^*]dxdy \tag{3.1}$$

Now for any TE mode

$$E_x = jk_y B' \cos k_x x \sin k_y y$$

$$E_y = -jk_x B' \sin k_x x \cos k_y y$$

$$H_x = -E_y/Z_{TE}$$

$$H_y = E_x/Z_{TE} \tag{3.2}$$

where

$$B' = \frac{\eta f}{k_c f_c} B \qquad Z_{TE} = \frac{E_T}{H_T} = \frac{\eta}{\sqrt{1 - (\lambda_0/\lambda_c)^2}}$$

$$k_x = \frac{m\pi}{a} \qquad \lambda_c = \frac{2\pi}{k_c} = \frac{2\pi}{\sqrt{k_x^2 + k_y^2}}$$

$$k_y = \frac{n\pi}{b}$$

Therefore,

$$W_z = \frac{1}{2}\int_0^b\int_0^a \mathrm{Re}\left[\frac{k_y^2 B'^2}{Z_{TE}} \cos^2 k_x x \sin^2 k_y y + \frac{k_x^2 B'^2}{Z_{TE}} \sin^2 k_x x \cos^2 k_y y\right] dxdy$$

$$= \frac{B'^2}{2Z_{TE}}\int_0^{n\pi}\int_0^{m\pi}\left[\left(\frac{k_y}{k_x}\right) \cos^2 k_x x \sin^2 k_y y + \left(\frac{k_x}{k_y}\right) \sin^2 k_x x \cos^2 k_y y\right] d(k_x x)d(k_y y) \tag{3.3}$$

$$(\text{if } m \neq 0) = \frac{B'^2}{2Z_{TE}} \int_0^{n\pi} \left[\left(\frac{a}{fm}\right)\left(\frac{m\pi}{2}\right) \sin^2 k_y y + \left(\frac{bm}{an}\right)\left(\frac{m\pi}{2}\right) \cos^2 k_y y \right] d(k_y y)$$

$$(\text{if } n \neq 0) = \frac{B'^2}{2Z_{TE}} \left[\left(\frac{an}{bm}\right)\left(\frac{m\pi}{2}\right)\left(\frac{n\pi}{2}\right) + \left(\frac{bm}{an}\right)\left(\frac{m\pi}{2}\right)\left(\frac{n\pi}{2}\right) \right] \tag{3.4}$$

$$W_z = \frac{ab\eta f^2 B^2}{8f_c^2} \sqrt{1 - (f_c/f)^2} \qquad (m \neq 0 \text{ and } n \neq 0) \quad \text{or}$$

$$= \frac{ab\eta f^2 B^2}{4f_c^2} \sqrt{1 - (f_c/f)^2} \qquad (m = 0 \text{ or } n = 0) \tag{3.5}$$

Now the amplitude squared term is

$$|E_x^{TE}|^2 = \frac{\eta^2 k_y^2 f^2 B^2}{k_c^2 f_c^2} = \eta^2 \left(\frac{n\pi}{b}\right)^2 \left(\frac{f}{f_c}\right)^2 \left(\frac{B}{k_c}\right)^2 \tag{3.6}$$

where

$$k_c = \left(\frac{2\pi f_c}{c}\right)^2 \qquad c = \frac{1}{\sqrt{\mu_0 \epsilon_0}} \qquad \eta = \sqrt{\mu_0/\epsilon_0}$$

Rearranging the amplitude squared equation

$$B^2 = \left(\frac{k_c}{\eta}\right)^2 \left(\frac{b}{n\pi}\right)^2 \left(\frac{f_c}{f}\right)^2 |E_x^{TE}|^2 \tag{3.7}$$

Therefore,

$$W_z^{TE} = \frac{ab^3 \epsilon_0}{2n^2 c} \sqrt{1 - (f_c/f)^2}\, |E_x^{TE}|^2 \qquad (m \text{ and } n \neq 0), \text{ or}$$

$$= \frac{ab^3 \epsilon_0}{n^2 c} \sqrt{1 - (f_c/f)^2}\, |E_x^{TE}|^2 \qquad (m \text{ or } n = 0) \tag{3.8}$$

Using the same procedure one can obtain W_z^{TM}.

One can now set up all the linear equations for the computer calculation. For the broad wall measurement

$$R_m = \frac{2}{p} \sum_{i=1}^{p-1} R_{yt}\left(\frac{ia}{p}\right) \sin\left(\frac{im\pi}{p}\right)$$

$$I_m = \frac{2}{p} \sum_{i=1}^{p-1} I_{yt}\left(\frac{ia}{p}\right) \sin\left(\frac{im\pi}{p}\right) \qquad (3.9)$$

where

$$R_{yt} = \left|E_{yt}\left(\frac{ia}{p}\right)\right| \cos\phi_t\left(\frac{ia}{p}\right),$$

$$I_{yt} = \left|E_{yt}\left(\frac{ia}{p}\right)\right| \sin\phi_t\left(\frac{ia}{p}\right),$$

$p = 1 + M_{max}$,

a = waveguide broadwall dimension.

For the narrow wall measurement,

$$R_n = \frac{2}{q} \sum_{j=1}^{q-1} R_{xt}\left(\frac{jb}{q}\right) \sin\left(\frac{jn\pi}{q}\right)$$

$$I_n = \frac{2}{q} \sum_{j=1}^{q-1} I_{xt}\left(\frac{jb}{q}\right) \sin\left(\frac{jn\pi}{q}\right) \qquad (3.10)$$

where

$$R_{xt} = \left|E_{xt}\left(\frac{jb}{q}\right)\right| \cos\phi_t\left(\frac{jb}{q}\right),$$

$$I_{xt} = \left|E_{xt}\left(\frac{jb}{q}\right)\right| \sin\phi_t\left(\frac{jb}{q}\right),$$

$q = 1 + N_{max}$,

b = waveguide narrow wall dimension.

One can set up the equations for each cross section for E_y for the third and second harmonics, respectively.

For the third harmonic, the eleven propagating modes are TE_{10}, TE_{20}, TE_{01}, TE_{11}, TM_{11}, TE_{21}, TM_{21}, TE_{30}, TM_{31}, TE_{31} and TE_{40}. As described earlier, there are four (M_{max}) broad wall probes in each of two ($N_d + 1$) rows spaced 3.8 cm apart. Now one has four [$2(N_d + 1)$] equations as follows

$$\left\{\begin{array}{l}
{}^1R_{ym0} + {}^1R_{ym1} + {}^0I_{ym0} + {}^0I_{ym} = {}^1R_{ym} = \frac{2}{p}\sum_{i=1}^{p-1} R_{yt1}\left(\frac{ia}{p}\right)\sin\left(\frac{imπ}{p}\right) \\
{}^0R_{ym0} + {}^0R_{ym1} + {}^1I_{ym0} + {}^1I_{ym1} = {}^1I_{ym} = \frac{2}{p}\sum_{i=1}^{p-1} I_{yt1}\left(\frac{ia}{p}\right)\sin\left(\frac{imπ}{p}\right) \\
\cos\theta_{m0}\,{}^1R_{ym0} + \cos\theta_{m1}\,{}^1R_{ym1} + \sin\theta_{m0}\,{}^1I_{ym0} + \sin\theta_{m1}\,{}^1I_{ym1} = {}^2R_{ym} = \frac{2}{p}\sum_{i=1}^{p-1} R_{yt2}\left(\frac{ia}{p}\right)\sin\left(\frac{imπ}{p}\right) \\
-\sin\theta_{m0}\,{}^1R_{ym0} - \sin\theta_{m1}\,{}^1R_{ym1} + \cos\theta_{m0}\,{}^1I_{ym0} + \cos\theta_{m1}\,{}^1I_{my1} = {}^2I_{ym} = \frac{2}{p}\sum_{i=1}^{p-1} I_{yt2}\left(\frac{ia}{p}\right)\sin\left(\frac{imπ}{p}\right)
\end{array}\right\} \qquad (3.11)$$

N_d is the highest n-index existing in degenerate mode pairs and in this case is unity. M_{max} is the highest m-index and in this case is 4. p is the number of segments in one row which needs to be $\geq 1 + M_{max}$ and in this case is 5. The left upper corner superscripts 1 and 2 are the indices of the rows. The m-index varies from 1 to 4.

$$R_{yt_1}\left[\frac{ia}{p}\right] = \left|E_{yt_1}\left[\frac{ia}{p}\right]\right| \cos\phi_{yt_1}\left[\frac{ia}{p}\right]$$

$$I_{yt_1}\left[\frac{ia}{p}\right] = \left|E_{yt_1}\left[\frac{ia}{p}\right]\right| \sin\phi_{yt_1}\left[\frac{ia}{p}\right]$$

$$R_{yt_2}\left[\frac{ia}{p}\right] = \left|E_{yt_2}\left[\frac{ia}{p}\right]\right| \cos\phi_{yt_2}\left[\frac{ia}{p}\right]$$

$$I_{yt_2}\left[\frac{ia}{p}\right] = \left|E_{yt_2}\left[\frac{ia}{p}\right]\right| \sin\phi_{yt_2}\left[\frac{ia}{p}\right] \qquad (3.12)$$

$\theta_{m0} = \beta_{m0} \cdot \Delta Z$ where $\Delta Z = 3.80$ cm

$\theta_{m1} = \beta_{m1} \cdot \Delta Z$

.

.

.

$\theta_{mn} = \beta_{mn} \cdot \Delta Z$

$$\beta_{mn} = \frac{\omega}{c}\sqrt{1 - (f_c/f)^2}$$

$$f_c = \frac{c}{2}\sqrt{(m/a)^2 + (n/b)^2}$$

When the previous set of equations are expressed in matrix form $[A]\,\vec{X} = \vec{B}$ they become

$$\begin{bmatrix} 1 & 1 & 0 & 0 \\ 0 & 0 & 1 & 1 \\ \cos\theta_{m0} & \cos\theta_{m1} & \sin\theta_{m0} & \sin\theta_{m1} \\ -\sin\theta_{m0} & -\sin\theta_{m1} & \cos\theta_{m0} & \cos\theta_{m1} \end{bmatrix} \begin{bmatrix} {}^1R_{ym0} \\ {}^1R_{ym1} \\ {}^1I_{ym0} \\ {}^1I_{ym1} \end{bmatrix} = \begin{bmatrix} {}^1R_{ym} \\ {}^1I_{ym} \\ {}^2R_{ym} \\ {}^2I_{ym} \end{bmatrix} \qquad (3.13)$$

For the second harmonic, the five propagating modes are TE_{10}, TE_{20}, TE_{01}, TE_{11} and TM_{11}. Only two (M_{max}) probes in each of two ($N_d + 1$) rows are required but since the measurement apparatus used for the third harmonic is available to us with extra probes we can obtain greater

accuracy. The equations take the same form as for the third harmonic, noting that now m varies from 1 to 2.

Thus far the treatment and equations have dealt only with the two rows of broad wall probes and the various E_y's. Similarly, one obtains a set of E_x equations for the second and third harmonics from the four narrow wall probe measurements.

There is one (= N_{max}) probe in each row and four (= $M_d + 1$) rows spaced 3.80 cm apart on the narrow wall. Therefore, one has eight [= $2(m_d + 1)$] simultaneous equations for the third harmonic as follows

$$
\left\{
\begin{array}{l}
{}^1R_{x0n} + {}^1R_{x1n} + {}^1R_{x2n} + {}^1R_{x3n} + 0\cdot{}^1I_{x0n} + 0\cdot{}^1I_{x1n} + 0\cdot{}^1I_{x2n} + 0\cdot{}^1I_{x3n} = {}^1R_{xn} \\
0\cdot{}^1R_{x0n} + 0\cdot{}^1R_{x1n} + 0\cdot{}^1R_{x2n} + 0\cdot{}^1R_{x2n} + {}^1I_{x0n} + {}^1I_{x1n} + {}^1I_{x2n} + {}^1I_{x3n} = {}^1I_{xn} \\
\cos\theta_{0n}{}^1R_{x0n} + \cos\theta_{1n}{}^1R_{x1n} + \cos\theta_{2n}{}^1R_{x2n} + \cos\theta_{3n}{}^1R_{x3n} + \sin\theta_{0n}{}^1I_{x0n} + \sin\theta_{1n}{}^1I_{x1n} + \sin\theta_{2n}{}^1I_{x2n} + \sin\theta_{3n}{}^1I_{x3n} = {}^2R_{xn} \\
-\sin\theta_{0n}{}^1R_{x0n} - \sin\theta_{1n}{}^1R_{x1n} - \sin\theta_{2n}{}^1R_{x2n} - \sin\theta_{3n}{}^1R_{x3n} + \cos\theta_{0n}{}^1I_{x0n} + \cos\theta_{1n}{}^1I_{x1n} + \cos\theta_{2n}{}^1I_{x2n} + \cos\theta_{3n}{}^1I_{x3n} = {}^2I_{xn} \\
\cos2\theta_{0n}{}^1R_{x0n} + \cos2\theta_{1n}{}^1R_{x1n} + \cos2\theta_{2n}{}^1R_{x2n} + \cos2\theta_{3n}{}^1R_{x3n} + \sin2\theta_{0n}{}^1I_{x0n} + \sin2\theta_{1n}{}^1I_{x1n} + \sin2\theta_{2n}{}^1I_{x2n} + \sin2\theta_{3n}{}^1I_{x3n} = {}^3R_{xn} \\
-\sin2\theta_{0n}{}^1R_{x0n} - \sin2\theta_{1n}{}^1R_{x1n} - \sin2\theta_{2n}{}^1R_{x2n} - \sin2\theta_{3n}{}^1R_{x3n} + \cos2\theta_{0n}{}^1I_{x0n} + \cos2\theta_{1n}{}^1I_{x1n} + \cos2\theta_{2n}{}^1I_{x2n} + \cos2\theta_{3n}{}^1I_{x3n} = {}^3I_{xn} \\
\cos3\theta_{0n}{}^1R_{x0n} + \cos3\theta_{1n}{}^1R_{x1n} + \cos3\theta_{2n}{}^1R_{x2n} + \sin3\theta_{3n}{}^1I_{x3n} + \sin3\theta_{0n}{}^1I_{x0n} + \sin3\theta_{1n}{}^1I_{x1n} + \sin3\theta_{2n}{}^1I_{x2n} + \sin3\theta_{3n}{}^1I_{x3n} = {}^4R_{xn} \\
-\sin3\theta_{0n}{}^1R_{x0n} - \sin3\theta_{1n}{}^1R_{x1n} - \sin3\theta_{2n}{}^1R_{x2n} - \sin3\theta_{3n}{}^1R_{x3n} + \cos3\theta_{0n}{}^1I_{x0n} + \cos3\theta_{1n}{}^1I_{x1n} + \cos3\theta_{2n}{}^1I_{x2n} + \cos3\theta_{3n}{}^1I_{x3n} = {}^4I_{xn}
\end{array}
\right\}
$$

(3.14)

Equations (3.14) expressed in the form [A] $\vec{X} = \vec{B}$ becomes

$$\begin{bmatrix} 1 & 1 & 1 & 1 & 0 & 0 & 0 & 0 \\ 0 & 0 & 0 & 0 & 1 & 1 & 1 & 1 \\ \cos\theta_{0n} & \cos\theta_{1n} & \cos\theta_{2n} & \cos\theta_{3n} & \sin\theta_{0n} & \sin\theta_{1n} & \sin\theta_{2n} & \sin\theta_{3n} \\ -\sin\theta_{0n} & -\sin\theta_{1n} & -\sin\theta_{2n} & -\sin\theta_{3n} & \cos\theta_{0n} & \cos\theta_{1n} & \cos\theta_{2n} & \cos\theta_{3n} \\ \cos2\theta_{0n} & \cos2\theta_{1n} & \cos2\theta_{2n} & \cos2\theta_{3n} & \sin2\theta_{0n} & \sin2\theta_{1n} & \sin2\theta_{2n} & \sin2\theta_{3n} \\ -\sin2\theta_{0n} & -\sin2\theta_{1n} & -\sin2\theta_{2n} & -\sin2\theta_{3n} & \cos2\theta_{0n} & \cos2\theta_{1n} & \cos2\theta_{2n} & \cos2\theta_{3n} \\ \cos3\theta_{0n} & \cos3\theta_{1n} & \cos3\theta_{2n} & \cos3\theta_{3n} & \sin3\theta_{0n} & \sin3\theta_{1n} & \sin3\theta_{2n} & \sin3\theta_{3n} \\ -\sin3\theta_{0n} & -\sin3\theta_{1n} & -\sin3\theta_{2n} & -\sin3\theta_{3n} & \cos3\theta_{0n} & \cos3\theta_{1n} & \cos3\theta_{2n} & \cos3\theta_{3n} \end{bmatrix} \times \begin{bmatrix} {}^{1}R_{x0n} \\ {}^{1}R_{x1n} \\ {}^{1}R_{x2n} \\ {}^{1}R_{x3n} \\ {}^{1}I_{x0n} \\ {}^{1}I_{x1n} \\ {}^{1}I_{x2n} \\ {}^{1}I_{x3n} \end{bmatrix} = \begin{bmatrix} {}^{1}R_{xn} \\ {}^{1}I_{xn} \\ {}^{2}R_{xn} \\ {}^{2}I_{xn} \\ {}^{3}R_{xn} \\ {}^{3}I_{xn} \\ {}^{4}R_{xn} \\ {}^{4}I_{xn} \end{bmatrix}$$

(3.15)

where n = 1 (N_{max}) and noting that the location of row number 1 on the narrow wall is the same as the row number 1 on the broad wall.

For the second harmonic one needs only one (= N_{max}) probe in each row and two (= $M_d + 1$) rows such that there are four [= $2(M_d + 1)$] simultaneous equations as follows

$$\left\{ \begin{array}{l} {}^{1}R_{0xn} + {}^{1}R_{x1n} + 0\,{}^{1}I_{x0n} + 0\,{}^{1}I_{x1n} = {}^{1}R_{xn} = \frac{2}{q} \sum_{j=1}^{q-1} R_{xt1}\left(\frac{jb}{q}\right) \sin\left(\frac{jn\pi}{q}\right) \\ 0\,{}^{1}R_{0xn} + 0\,{}^{1}R_{x1n} + {}^{1}I_{x0n} + {}^{1}I_{x1n} = {}^{1}I_{xn} = \frac{2}{q} \sum_{j=1}^{q-1} I_{xb1}\left(\frac{jb}{q}\right) \sin\left(\frac{jn\pi}{q}\right) \\ \cos\theta_{0n}\,{}^{1}R_{0xn} + \cos\theta_{1n}\,{}^{1}R_{x1n} + \sin\theta_{0n}\,{}^{1}I_{x0n} + \sin\theta_{1n}\,{}^{1}I_{x1n} = {}^{2}R_{xn} = \frac{2}{q} \sum_{j=1}^{q-1} R_{xt2}\left(\frac{jb}{q}\right) \sin\left(\frac{jn\pi}{q}\right) \\ -\sin\theta_{0n}\,{}^{1}R_{0xn} - \sin\theta_{1n}\,{}^{1}R_{x1n} + \cos\theta_{0n}\,{}^{1}I_{x0n} + \cos\theta_{1n}\,{}^{1}I_{x1n} = {}^{2}I_{xn} = \frac{2}{q} \sum_{j=1}^{q-1} I_{xt2}\left(\frac{jb}{q}\right) \sin\left(\frac{jn\pi}{q}\right) \end{array} \right\}$$

(3.16)

or in matrix form $[A]\,\vec{X} = \vec{B}$

$$\begin{bmatrix} 1 & 1 & 0 & 0 \\ 0 & 0 & 1 & 1 \\ \cos\theta_{0n} & \cos\theta_{1n} & \sin\theta_{0n} & \sin\theta_{1n} \\ -\sin\theta_{0n} & -\sin\theta_{1n} & \cos\theta_{0n} & \cos\theta_{1n} \end{bmatrix} \begin{bmatrix} {}^{1}R_{x0n} \\ {}^{1}R_{x1n} \\ {}^{1}I_{x0n} \\ {}^{1}I_{x1n} \end{bmatrix} = \begin{bmatrix} {}^{1}R_{xn} \\ {}^{1}I_{xn} \\ {}^{2}R_{xn} \\ {}^{2}I_{xn} \end{bmatrix} \tag{3.17}$$

where M_d is the highest m-index existing in a degenerate mode pair which in this case is unity. N_{max} is the maximum n-index which in this case is unity. $q = 1 + N_{max}$ is the number of segments in one row and in this case is 2. The left upper corner superscripts 1 and 2 are the indices of the rows, noting that 1 refers to the same cross section as 1 on the broad wall. Also $n = 1(N_{max})$. As before with the broad wall data

$$\begin{aligned} R_{xt_1}\left(\frac{jb}{q}\right) &= \left|E_{xt_1}\left(\frac{jb}{q}\right)\right| \cos\phi_{xt_1}\left(\frac{jb}{q}\right) \\ R_{xt_2}\left(\frac{jb}{q}\right) &= \left|E_{xt_1}\left(\frac{jb}{q}\right)\right| \cos\phi_{xt_2}\left(\frac{jb}{q}\right) \\ I_{xt_1}\left(\frac{jb}{q}\right) &= \left|E_{xt_1}\left(\frac{jb}{q}\right)\right| \sin\phi_{xt_1}\left(\frac{jb}{q}\right) \\ I_{xt_2}\left(\frac{jb}{q}\right) &= \left|E_{xt_2}\left(\frac{jb}{q}\right)\right| \sin\phi_{xt_2}\left(\frac{jb}{q}\right) \end{aligned} \tag{3.18}$$

θ_{mn}, β_{mn} and f_c are the same as before.

To calculate the degenerate mode pairs one can use the following as before

$$(R_y^{TM})_{mn} = \frac{R_{ymn} + (1/q)R_{xmn}}{1 + (1/q)^2}$$

$$(R_y^{TE})_{mn} = \frac{R_{ymn} - qR_{xmn}}{1 + q^2}$$

$$(I_y^{TM})_{mn} = I_{ymn} + (1/q)I_{xmn}$$

$$(I_y^{TE})_{mn} = \frac{I_{ymn} - qI_{xmn}}{1 + q^2} \qquad (3.19)$$

where $q = na/mb$.

Finally we have the electric field amplitudes and relative phases

$$|E_y^{TM}|^2 = |R_y^{TM}|^2 + |I_y^{TM}|^2$$

$$|E_y^{TE}|^2 = |R_y^{TE}|^2 + |I_y^{TE}|^2$$

$$\phi^{TM} = \tan^{-1}\left[\frac{I_y^{TM}}{R_y^{TM}}\right]$$

$$\phi^{TE} = \tan^{-1}\left[\frac{I_y^{TE}}{R_y^{TE}}\right] \qquad (3.20)$$

5. CHECKING THE COMPUTER PROGRAM

It was necessary to devise a relatively simple check on the complex computer program. Using the calibration data for the probes, the P_i's for each of the eleven probes were calculated assuming one watt of power propagating with single mode purity. This was done for each of the five modes at the second harmonic and each of the eleven modes at the third harmonic. This requires eleven each amplitude and phase values for each pure mode at each harmonic or 352 values of P_i. Some debugging of the program was required.

For propagating TE modes the power is given by[6]

$$W_z^{TE} = \frac{\eta^2(f/f_c)^2}{2Z_{TE}} \int_{c.s.} H_z^2 dS = \frac{\eta^2(f/f_c)^2}{2Z_{TE}} B^2 \int_0^a \int_0^b \cos^2 k_x x \cos^2 k_y y \, dy dx \tag{4.1}$$

which becomes

$$W_z^{TE} = \frac{E_{y0}^2}{8Z_{TE}}\left(\frac{k_c}{k_x}\right)^2 ab = \frac{E_{x0}^2}{8Z_{TE}}\left(\frac{k_c}{k_y}\right)^2 ab \qquad \text{for } m \neq 0,\ n \neq 0$$

$$\frac{E_{y0}^2}{4Z_{TE}}\left(\frac{k_c}{k_x}\right)^2 ab \qquad \text{for } m \neq 0,\ n = 0$$

$$\frac{E_{x0}^2}{4Z_{TE}}\left(\frac{k_c}{k_x}\right)^2 ab \qquad \text{for } m = 0,\ n \neq 0 \quad . \tag{4.2}$$

For propagating TM modes

$$W_z^{TM} = \frac{Z_{TM}}{2\eta^2}\left(\frac{f}{f_c}\right)^2 \int_{c.s.} E_z^2 dS$$

$$= \frac{Z_{TM}}{2\eta^2}\left(\frac{f}{f_c}\right)^2 A^2 \int_0^a \int_0^b \sin^2 k_x x \sin^2 k_y y \, dy dx \tag{4.3}$$

which becomes

$$W_z^{TM} = \frac{E_{yo}^2}{8Z_{TM}}\left(\frac{k_c}{k_y}\right)^2 ab = \frac{E_{xo}^2}{8Z_{TM}}\left(\frac{k_c}{k_x}\right)^2 ab \qquad \text{for } m \neq 0,\ n \neq 0$$

$$= \frac{E_{yo}^2}{4Z_{TM}}\left(\frac{k_c}{k_y}\right)^2 ab \qquad \text{for } m = 0,\ n \neq 0$$

$$= \frac{E_{xo}^2}{4Z_{TM}}\left(\frac{k_c}{k_x}\right)^2 ab \qquad \text{for } m \neq 0,\ n = 0 \tag{4.4}$$

where

$$k_x = \frac{m\pi}{a} \qquad k_y = \frac{n\pi}{b} \qquad k_c^2 = k_x^2 + k_y^2 = \left(\frac{2\pi f_c}{c}\right)^2$$

$$B = \frac{E_{yo}}{\eta}\left(\frac{f_c}{f}\right)\left(\frac{k_c}{k_x}\right) = \frac{E_{xo}}{\eta}\left(\frac{f_c}{f}\right)\left(\frac{k_c}{k_y}\right)$$

$$A = \frac{E_{yo}}{Z_{TM}}\left(\frac{f_c}{f}\right)\left(\frac{k_c}{k_y}\right) = \frac{E_{xo}}{Z_{TM}}\left(\frac{f_c}{f}\right)\left(\frac{k_c}{k_x}\right)$$

$$Z_{TE} = \frac{\eta}{\sqrt{1 - (f_c/f)^2}} \qquad Z_{TM} = \eta\sqrt{1 - (f_c/f)^2}$$

The electric field configurations, k_x, k_y and k_c are summarized in Table 2.

REFERENCES

1. M. P. Forrer and K. Tomiyasu, "Determination of higher order propagating modes in waveguide systems," J. Appl. Phys., Vol. 29, pp 1040-1045, July 1958.
2. V. G. Price, "Measurement of harmonic power generated by microwave transmitters," IRE Trans. on Microwave Theory and Techniques, Vol. MTT-7, pp 116-120, January 1959.
3. D. J. Lewis, "Mode couplers and multimode measurement techniques," IRE Trans. on microwave theory and techniques," Vol. MTT-7, pp 110-116, January 1959.
4. E. D. Sharp and E.M.T. Jones, "A sampling measurement of multimode waveguide power," IRE Trans. on Microwave Theory and Techniques, Vol. MTT-10, pp 73-82, January 1962.
5. J. J. Taub, "A new technique for multimode power measurement," IRE Trans. on Microwave Theory and Techniques, Vol. MTT-10, pp 496-505, November 1962.
6. S. Ramo and J. R. Whinnery, Fields and Waves in Modern Radio (John Wiley and Sons, Inc., New York, 1958) pp 344-367.

Table I. Multimode Power Distribution for a SLAC High Power Klystron in Watts (Peak)

Tube: M-413

Propagating Mode	Fundamental 2856 MHz	Second Harmonic 5712 MHz	Third Harmonic 8568 MHz
TE_{10}	31.0×10^6	11,206	269
TE_{20}		1,130	1,490
TE_{01}		52,570	754
TE_{11}		50,643	188
TM_{11}		8,261	450
TE_{21}			258
TM_{21}			174
TE_{30}			138
TE_{31}			93
TM_{31}			37
TE_{40}			42
TOTAL	31.0×10^6 (0 db Ref.)	123,810 (-24.0 db)	3,894 (-39.0 db)

Table II. E Field Summary

	E_y	E_x	K_x	K_y	K_c
TE_{10}	$E_{yo} \sin\frac{\pi x}{a}$	0	$\frac{\pi}{a}$	0	$\frac{\pi}{a}$
TE_{20}	$E_{yo} \sin\frac{2\pi x}{a}$	0	$\frac{2\pi}{a}$	0	$\frac{2\pi}{a}$
TE_{30}	$E_{yo} \sin\frac{3\pi x}{a}$	0	$\frac{2\pi}{a}$	0	$\frac{3\pi}{a}$
TE_{40}	$E_{yo} \sin\frac{4\pi x}{a}$	0	$\frac{4\pi}{a}$	0	$\frac{4\pi}{a}$
TE_{11}	$E_{yo} \sin\frac{\pi x}{a} \cos\frac{\pi y}{b}$	$E_{xo} \cos\frac{\pi x}{a} \sin\frac{\pi y}{b}$	$\frac{\pi}{a}$	$\frac{\pi}{b}$	$\pi\sqrt{\frac{1}{a^2}+\frac{1}{b^2}}$
TE_{21}	$E_{yo} \sin\frac{2\pi x}{a} \cos\frac{\pi y}{b}$	$E_{xo} \cos\frac{2\pi x}{a} \sin\frac{\pi y}{b}$	$\frac{2\pi}{a}$	$\frac{\pi}{b}$	$\pi\sqrt{\frac{4}{a^2}+\frac{1}{b^2}}$
TE_{31}	$E_{yo} \sin\frac{3\pi x}{a} \cos\frac{\pi y}{b}$	$E_{xo} \cos\frac{3\pi x}{a} \sin\frac{\pi y}{b}$	$\frac{3\pi}{a}$	$\frac{\pi}{b}$	$\pi\sqrt{\frac{9}{a^2}+\frac{1}{b^2}}$
TE_{01}	0	$E_{xo} \sin\frac{\pi y}{b}$	0	$\frac{\pi}{b}$	$\frac{\pi}{b}$
TM_{11}	$E_{yo} \sin\frac{\pi x}{a} \cos\frac{\pi y}{b}$	$E_{xo} \cos\frac{\pi x}{a} \sin\frac{\pi y}{b}$	$\frac{\pi}{a}$	$\frac{\pi}{b}$	$\pi\sqrt{\frac{1}{a^2}+\frac{1}{b^2}}$
TM_{21}	$E_{yo} \sin\frac{2\pi x}{a} \cos\frac{\pi y}{b}$	$E_{xo} \cos\frac{2\pi x}{a} \sin\frac{\pi y}{b}$	$\frac{2\pi}{a}$	$\frac{\pi}{b}$	$\pi\sqrt{\frac{4}{a^2}+\frac{1}{b^2}}$
TM_{31}	$E_{yo} \sin\frac{3\pi x}{a} \cos\frac{\pi y}{b}$	$E_{xo} \cos\frac{3\pi x}{a} \sin\frac{\pi y}{b}$	$\frac{3\pi}{a}$	$\frac{\pi}{b}$	$\pi\sqrt{\frac{9}{a^2}+\frac{1}{b^2}}$

FIGURE CAPTIONS

Fig. 1. Detail of single electric field probe assembly.

Fig. 2. Multiprobe/cable assembly.

Fig. 3. Simplified block diagram – low power amplitude and phase calibration.

Fig. 4. Simplified block diagram – high power measurement.

Fig. 5. Waveguide coordinate system orientation.

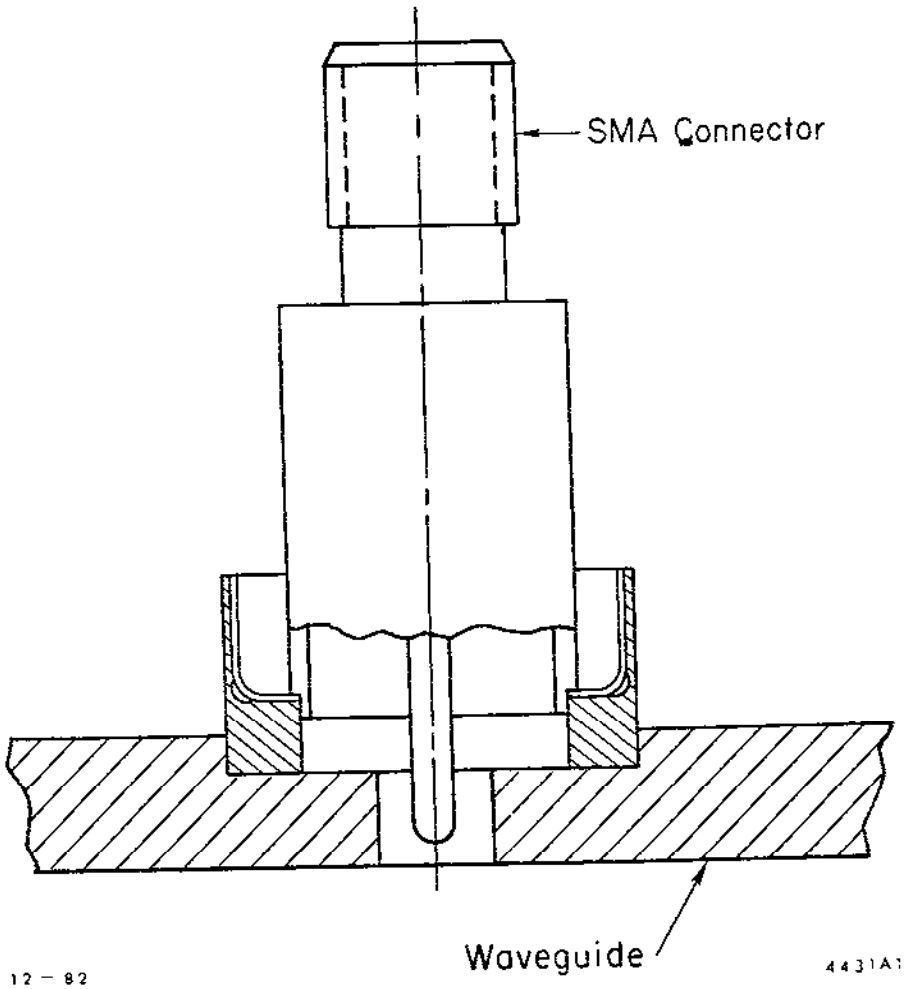

Fig. 1

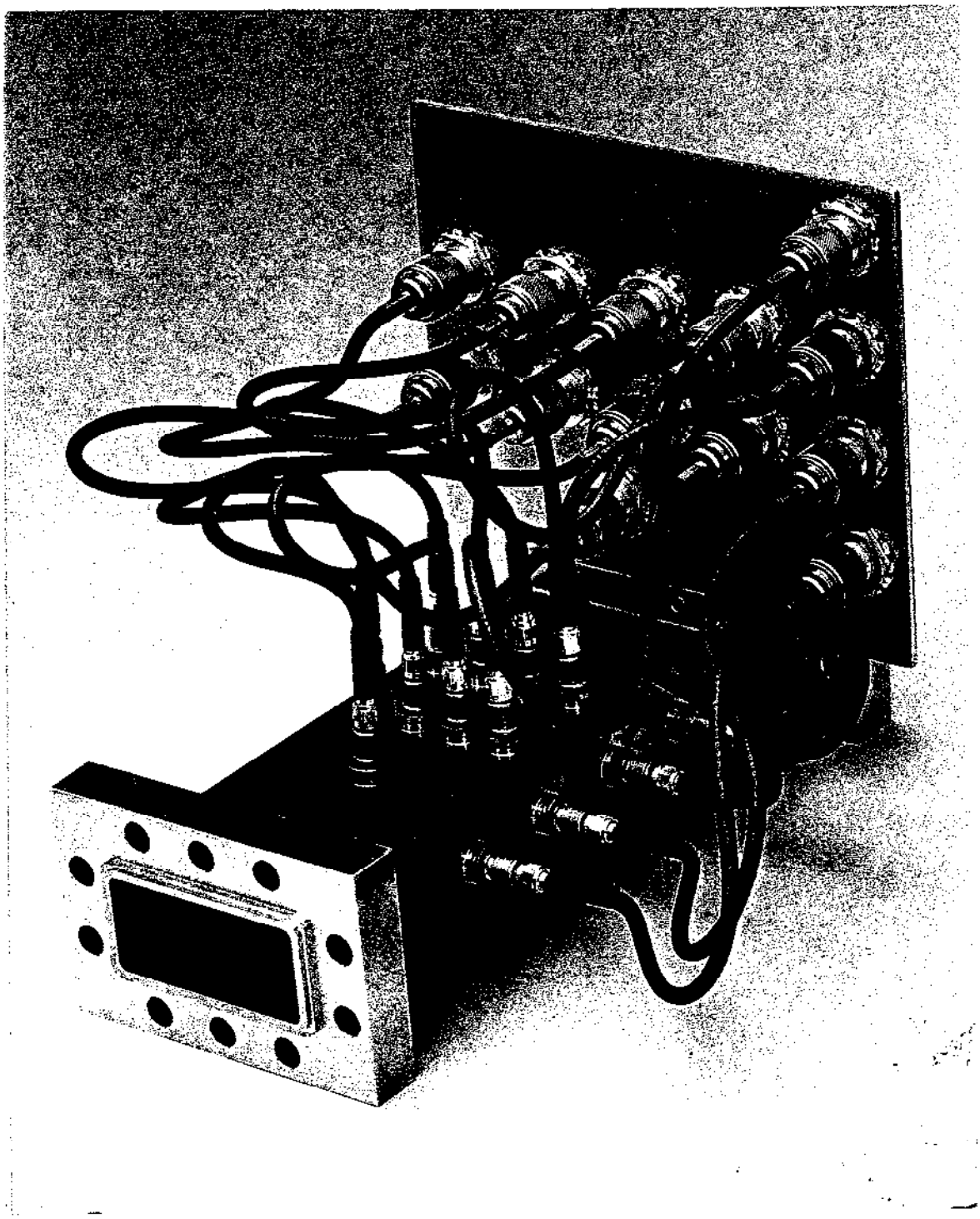

FIGURE 2

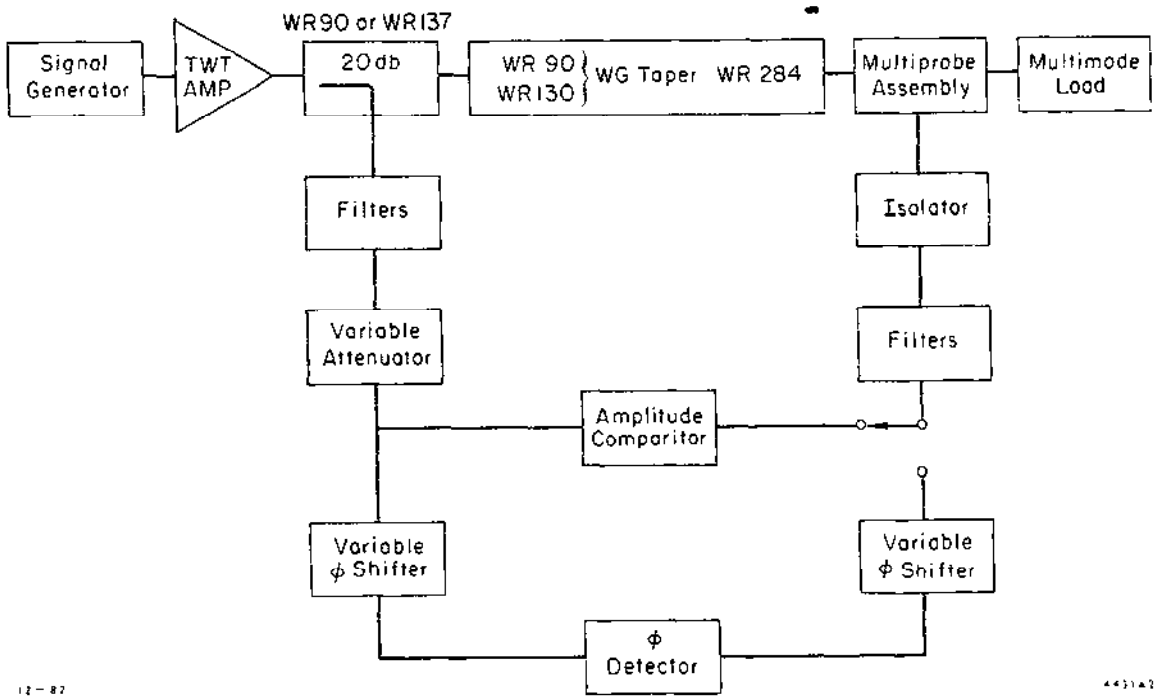
WR90 or WR137
Signal Generator
TWT AMP
20db
WR 90
WR130
WG Taper WR 284
Multiprobe Assembly
Multimode Load
Filters
Isolator
Variable Attenuator
Filters
Amplitude Comparitor
Variable ϕ Shifter
Variable ϕ Shifter
ϕ Detector

Fig. 3

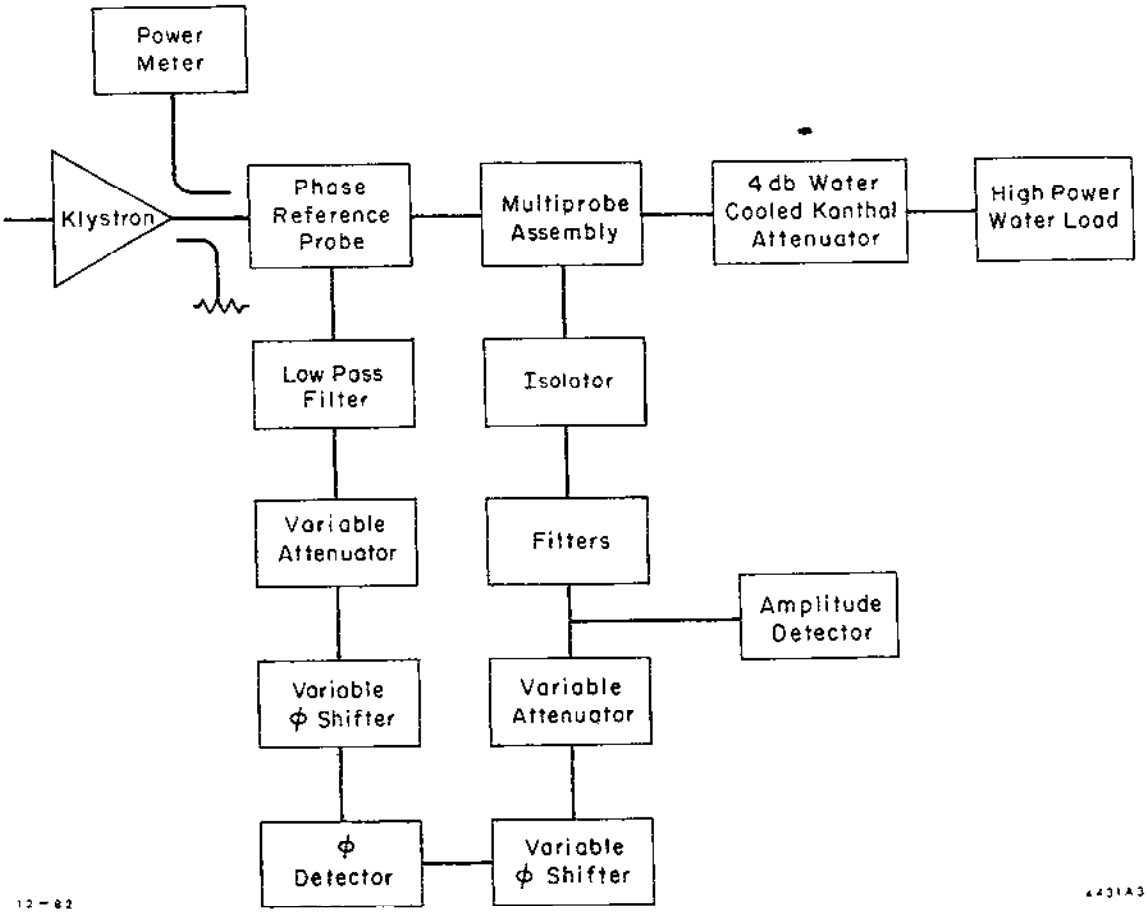
Power Meter
Klystron
Phase Reference Probe
Multiprobe Assembly
4 db Water Cooled Kanthal Attenuator
High Power Water Load
Low Pass Filter
Isolator
Variable Attenuator
Filters
Amplitude Detector
Variable ϕ Shifter
Variable Attenuator
ϕ Detector
Variable ϕ Shifter
12-82
4431A3

Fig. 4

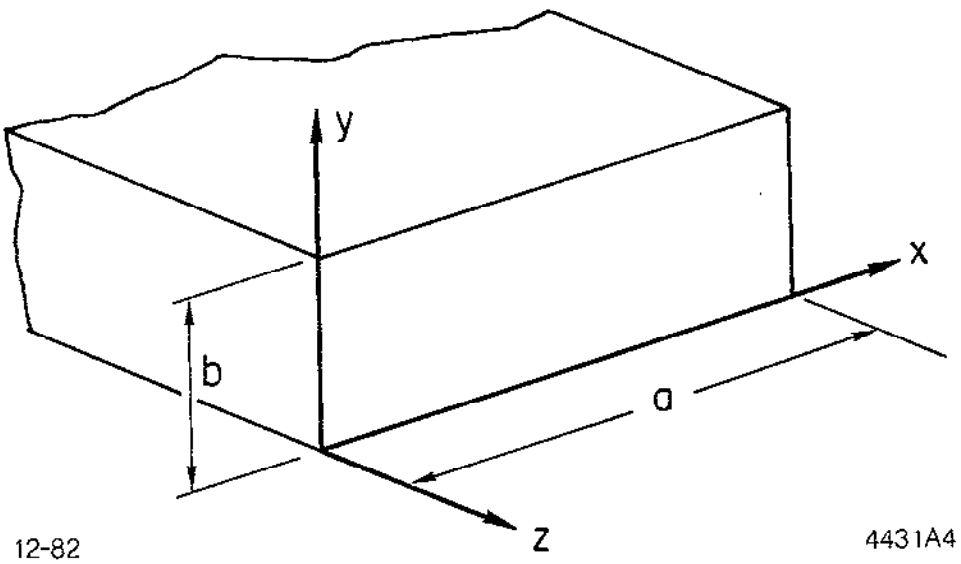

Fig. 5